Magnetoelectricity of single molecular toroics: The Dy_4 ring cluster

A. I. Popov,[1,2,*] D. I. Plokhov,[3,†] and A. K. Zvezdin[1,3,‡]

[1]*Moscow Institute of Physics and Technology, 9 Institutsky Pereulok, 141700, Dolgoprudny, Moscow region, Russia*

[2]*National Research University of Electronic Technology, Building 1, Shokin Square, 124498, Zelenograd, Moscow, Russia*

[3]*A. M. Prokhorov General Physics Institute of Russian Academy of Sciences, 38 Vavilov Street, 119991, Moscow, Russia*

(Received 20 June 2015; revised manuscript received 1 August 2016; published 9 November 2016)

Spin-electric interactions and magnetic and magnetoelectric properties of the Dy_4 ring molecular nanocluster are investigated. The effective spin-electric Hamiltonian is derived on a base of developed quantum mechanical model of the cluster spin structure. It is shown that the toroidal moment is a source of the quantum magnetoelectric effect. The dynamics of the toroidal moment (macroscopic quantum tunneling) is also discussed.

DOI: 10.1103/PhysRevB.94.184408

I. INTRODUCTION

Metal-organic molecular nanomagnets (so-called single molecular magnets, SMMs) are the focus of intense research at the fascinating point where quantum mechanics meets the classical world. Such mesoscopic objects are a source of novel physical effects, and they inspire the development of profound theories and prospective applications.

The most impressive phenomenon in the physics of SMMs is the macroscopic quantum tunneling (MQT) of magnetization, which has developed into a subject of great interest after the introduction of the concept by Caldeira and Leggett in the beginning of the 1980s [1]. In this context, single molecular magnets constitute the model system that best allows the observation of quantum tunneling of the magnetization, thermally assisted quantum tunneling, and resonant tunneling of the magnetic moment [2].

The most well known molecule of this type is Mn_{12}-ac. This molecule is composed of twelve interacting manganese ions and has the $S = 10$ total spin ground state with high uniaxial anisotropy. Well isolated from each other, the molecules present a superparamagnetic behavior above a blocking temperature of about 3 K [3], and a temperature-dependent hysteresis with distinctive steps, owing to the thermally assisted resonant quantum tunneling of the magnetization [2]. Below 1 K these steps become temperature independent as pure quantum tunneling turns to be the dominant reversal process [4–6]. The Hamiltonian with complex anisotropy contributions combined with the Landau-Zener model [7] has been used to explain the experimental results, but there are still some controversies surrounding experimental results and theoretical predictions despite the large amount of publications [8].

The induction of SMMs into the field of quantum computing [9] has yielded a variety of theoretical possibilities for the implementation of a quantum computer [10]. Although the vast majority of research that has been done in the field is purely theoretical, most of the proposals rely on solid experimental observations that reside in both classical and quantum domains. The proposed mechanisms for using molecular magnets as qubits are all based, at least in part, on the quantum phenomenon of spin tunneling and the interaction of a magnetically anisotropic molecule with external magnetic fields [11]. This fundamental manipulation leads to the theoretical realization of quantum gates and data storage using the Grover algorithm [12], which improves on the classical database search. SMMs are also promising objects for use in the development of molecular spintronics [13].

Molecular magnets have several advantages, such as uniform nanoscale size, solubility in organic solvents, readily alterable peripheral ligands helping to tune their properties finely, possibility of directed assembly or self assembly, etc. Nevertheless, there are some disadvantages; the most obstructive are the inability to scale to arbitrarily high spins, the presence of strong decoherence to classical physics, and the extreme temperature dependence of almost all characteristics of a molecular magnetic qubit. These limitations make experimental research papers on the use of molecular magnets for quantum computing be few and far between, with the vast majority examining physical properties of systems.

All these limitations are rooted in the very idea of spin state control with magnetic fields. In recent years, however, a new trend of spin manipulation by electrical means (electric fields or/and electric currents) has gained a foothold because of the much better ability to localize electric fields compared to magnetic ones [14]. There are a number of papers [15,16] dedicated to investigation of systems driven by spin-electric interaction. The pull is owed to the presence of another degree of freedom, the toroidal moment, which couples with an electric field (or an electric current), which is thus nonsensitive to the influence of stray magnetic fields [17]. It should also be noted that the presence of the toroidal moment in a system gives a wonderful opportunity to observe the quantum magneto-electric effect (MEE) in it.

From this point of view, metal-organic molecules with a ring rare-earth ion core are of significant importance. Such an ordering can naturally be described in terms of toroidal moment, and the presence of rare-earth ions enhances the magnetoelectricity to a great extent [18]. A whole series of dysprosium-based ring molecular nanoclusters (Dy_3 [19], Dy_4 [20], and Dy_6 [21]) has recently been synthesized. Other studies mostly focus on either changing the lanthanide ion while keeping the ligand system constant or changing the ligand but keeping the coordination sphere around the lanthanide ion identical in multilanthanide systems; see Ref. [22] and references therein.

*aip_2001@mail.ru

†dmitry.plokhov@gmail.com

‡zvezdin@gmail.com

A few years ago, the question of the toroidal moment existence in the triangular Dy_3 cluster, the progenitor of the family, was discussed [19,23]. The dynamics of the toroidal moment [24] and magnetoelectric properties of molecular crystal Dy_3 have also been investigated [25]. It is remarkable that the dynamics has a number of similar features that are characteristic for the dynamics of the magnetic moment in single molecular magnets (SMMs). By analogy, the ring clusters can be called single molecular toroics (SMTs).

It is believed that SMTs have all the advantages of SMMs, and the presence of the toroidal moment in SMTs reduces several disadvantages of SMMs. The SMTs seem to be most promising for future applications in quantum computing and information storage as molecular multiferroic materials with magnetoelectric effects. The key features offering advantages are their insensitivity to external homogeneous magnetic fields, remarkably weak magnetic interaction among themselves, and the possibility to manipulate the toroidal states by electrical means (electric currents or variable electric fields). In this interdisciplinary research area that spans chemistry, physics, and material sciences, synthetic chemists have already produced SMT systems suitable for detailed experimental study, while *ab initio* calculations have proven their reliability in the description of toroidal magnetization; see Refs. [26] and [27] for recent reviews and Ref. [28] for the book on the subject. Lanthanide-based ring complexes with the high symmetry of the molecule unit and strong intermetallic dipolar interactions with strong axial anisotropy on the metal sites are the most promising route toward the design of efficient SMTs.

The present work is devoted to the comprehensive investigation of dysprosium-based SMTs by example of Dy_4 ring molecular nanoclusters. We describe the structure of the systems and determine the hierarchy of interactions in them; see Sec. II. In Sec. III, the magnetic properties of the Dy_4 molecular cluster are depicted. The dependencies of the magnetization on the magnetic field and temperature are obtained. Then, we proceed to the magnetoelectricity of the system. The spin-electric Hamiltonian is derived in Sec. IV and the magnetoelectric effect is described. Finally, we discuss some questions of the toroidal moment dynamics, especially the phenomenon of macroscopic quantum tunneling of the toroidal moment; see Sec. V.

II. THE MODEL OF THE Dy_4 CLUSTER

First of all, we should describe the inner structure of the Dy_4 molecular cluster and formulate the model Hamiltonian. Because magnetic and magnetoelectric properties of the cluster are owed to the presence of Dy^{3+} ions, we will focus on the dysprosium ion core.

Let the abscissa axis of the $OXYZ$ laboratory coordinate system be directed along the longer diagonal of the parallelogram formed by the dysprosium ions, as shown in Fig. 1. Supposing that the magnetization axes of the ions are the $\mathbf{e}_z(i)$ local axes, we present the orientations of the local coordinate axes of the ions with respect to the laboratory frame,

$$\begin{aligned}
\mathbf{e}_z(3) &= \mathbf{e}_X \cos\delta + \mathbf{e}_Y \sin\delta,\\
\mathbf{e}_x(3) &= \mathbf{e}_X \sin\delta - \mathbf{e}_Y \cos\delta,\\
\mathbf{e}_z(4) &= \mathbf{e}_Y \cos\gamma - \mathbf{e}_X \sin\gamma,\\
\mathbf{e}_x(4) &= \mathbf{e}_Y \sin\gamma + \mathbf{e}_X \cos\gamma,\\
\mathbf{e}_\alpha(1) &= -\mathbf{e}_\alpha(3),\\
\mathbf{e}_\alpha(2) &= -\mathbf{e}_\alpha(4).
\end{aligned}$$

Here δ and γ stand for the small angles between the laboratory abscissa axis and unit vectors $\mathbf{e}_z(3)$ and $\mathbf{e}_x(4)$, relatively (see Fig. 1). For the purpose of brevity, we will also denote $\mathbf{e}_z(3)$ as $\mathbf{l}_1$ and $\mathbf{e}_z(4)$ as $\mathbf{l}_2$.

Since the Dy_4 ion core is put together from the Ising-type Dy^{3+} ions, the Hamiltonian of the cluster can be represented

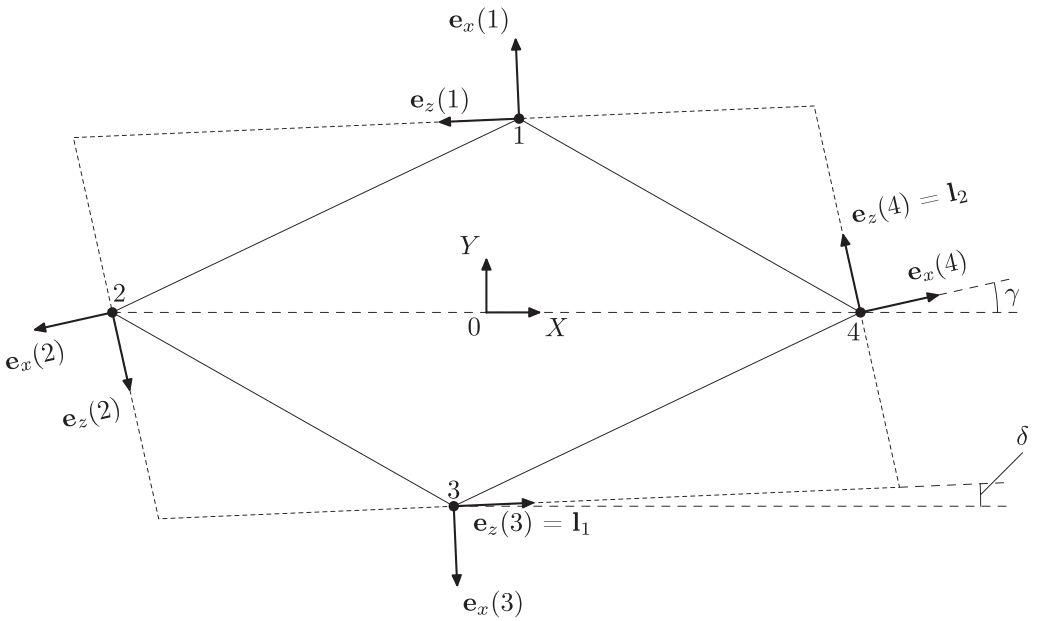

FIG. 1. The ion core of the Dy_4 molecular cluster depicted with respect to the laboratory OXY frame. Here $\mathbf{e}_z(i)$, $i = 1,2,3,4$, are directed along the ion magnetization axes.

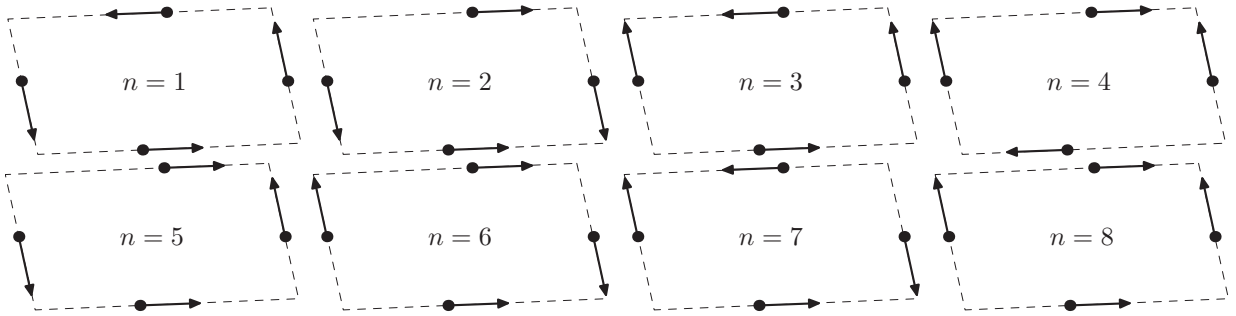

FIG. 2. The ground ($n = 1$) and excited ($n = 2 \ldots 8$) spin configurations in the Dy_4 cluster, the Kramers-conjugate states with $n = 9 \ldots 16$ (not shown) have all the spins reversed. For the energies, total spin, and toroidal moment of the configurations, see Table I.

in a form of an exchange Hamiltonian [20,29],

$$\mathcal{H}_0 = -J_1(S_{1z}S_{4z} + S_{3z}S_{2z}) - J_2(S_{1z}S_{2z} + S_{3z}S_{4z}) - J_3 S_{1z}S_{3z} - J_4 S_{2z}S_{4z}, \quad (1)$$

where S_{iz} are the projection operators of the effective spin onto the $\mathbf{e}_z(i)$ local axes, and the corresponding quantum numbers are $S_{iz} = \pm 1/2$. The values of the effective exchange constants J_k can be taken from Ref. [20], $J_1 = 4.44$ cm^{-1}, $J_2 = 1.22$ cm^{-1}, $J_3 = 3.09$ cm^{-1}, and $J_4 = 0.42$ cm^{-1}.

Figure 2 shows eight of the sixteen possible spin configurations of the dysprosium ions in a Dy_4 cluster; the corresponding energies E_{n0} are calculated from Eq. (1) and given in Table I. The other eight configurations can be obtained by reversing all dysprosium ion spins. Of course, the energies of the reversed configurations are the same.

The spin ordering of the Dy_4 nanocluster can be characterized in terms of spin chirality [20,29]. It is clear that spins in the ground states ($n = 1$ and $n = 9$) are inversely twisted; i.e., the states have the opposite chirality. The natural physical quantity associated with spin chirality in this case in the T-odd polar vector of a toroidal (anapole) moment, which corresponds to the first term in the toroidal (anapole) multipole expansion of an arbitrary electric current distribution. It reads as

$$\mathbf{T} = \frac{1}{10c}\int [(\mathbf{jr})\mathbf{r} - 2r^2\mathbf{j}]d^3\mathbf{r},$$

where $\mathbf{j}(\mathbf{r},t)$ is the electric current density [30]. In the case of the dysprosium cluster, then we deal with localized magnetic moments, and the expression can be transferred to

$$\mathbf{T} = \frac{1}{2} g_J \mu_B \sum_i [\mathbf{r}_i \times \mathbf{J}_i],$$

where $\mathbf{r}_i$ and $\mathbf{J}_i$ are the radius vector and the total angular momentum of the ith ion, respectively, g_J stands for the Lande factor, and μ_B is the Bohr magneton.

The values of dimensionless toroidal moments $\tau = T_Z/T_0$ with $T_0 = \frac{15}{4} g_J \mu_B d_1$ in different spin configurations at $T = 0$ K are given in Table I. Here d_1 and d_2 are the lengths of the shorter and the longer diagonals of the parallelogram formed by the dysprosium ions, respectively, $d_2/d_1 = q > 1$, and ε is a small angle between the shorter diagonal and the laboratory ordinate axis. Obviously, the τ_n values differ in sign for conjugate states.

III. THE MAGNETIC PROPERTIES OF THE Dy_4 CLUSTER

The expression for the energy levels in a nonzero magnetic field of the dysprosium cluster reads

$$E_n(H) = E_{n0} \pm \mu \mathbf{m}_n \mathbf{H}, \quad (2)$$

where E_{n0} are the zero-field energy levels, $\mu = 15\mu_B g_J$, and $g_J = \frac{4}{3}$. The cluster total effective spin $\mathbf{m}_n = \mathbf{M}_n/2\mu$ is given by

$$\mathbf{m}_n = \sum_{i=1}^{4} \langle \mathbf{S}_{iz} \rangle_n = \frac{1}{2}\sum_{i=1}^{4} \sigma_n(i)\mathbf{e}_z(i), \quad (3)$$

where symbol $\sigma_n(i)$ denotes the sign of the ith ion spin projection onto the $\mathbf{e}_z(i)$ axis for the nth spin configuration. The $\mathbf{m}_n$ vectors are listed in Table I. The corresponding energy diagram is shown in Fig. 3.

It is clear that in the absence of a magnetic field the ground state has zero toroidal moment because of degeneration. If a magnetic field is applied, the minimal level crossing field

TABLE I. The energies and dimensionless values of the magnetic $\mathbf{m}$ and toroidal τ moments of the spin configurations in a Dy_4 cluster at $T = 0$ K.

n	E_{n0} (cm^{-1})	$\mathbf{m}_n = \frac{\mathbf{M}_n}{2\mu}$, $\mu = 15 g_J \mu_B$, $g_J = \frac{4}{3}$	$\tau_n = \frac{T_n}{T_0}$, $T_0 = \frac{1}{4}\mu d_1$
1	0	0	$\cos(\varepsilon + \delta) + q\cos\gamma$
2	2.967	$\mathbf{l}_1 - \mathbf{l}_2$	0
3	3.033	$\mathbf{l}_2$	$\cos(\varepsilon + \delta)$
4	3.033	$\mathbf{l}_2$	$-\cos(\varepsilon + \delta)$
5	4.365	$\mathbf{l}_1$	$q\cos\gamma$
6	4.365	$\mathbf{l}_1$	$-q\cos\gamma$
7	5.639	0	$\cos(\varepsilon + \delta) - q\cos\gamma$
8	6.191	$\mathbf{l}_1 + \mathbf{l}_2$	0

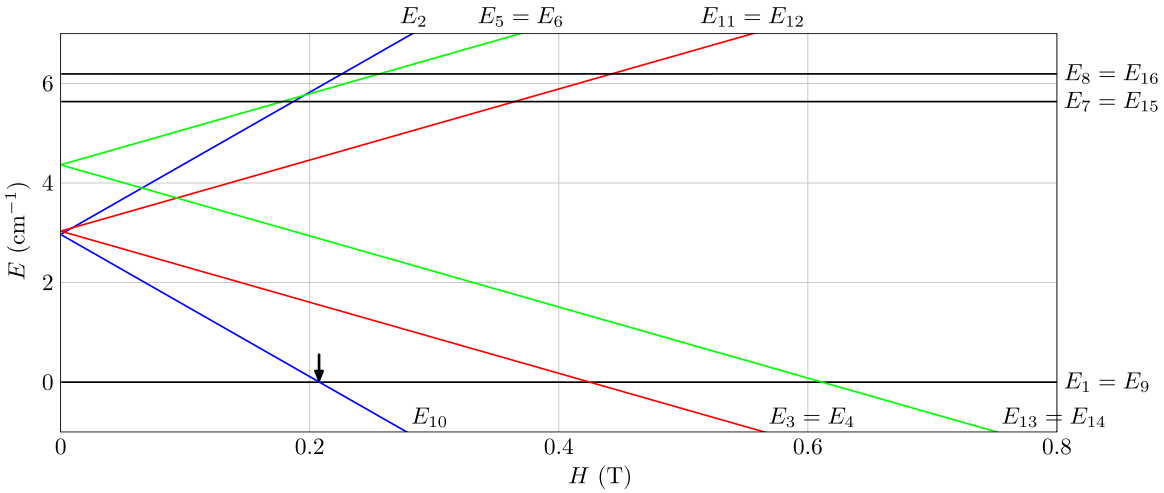

FIG. 3. The energy diagram of the Dy_4 cluster in magnetic field **H** directed along the $\mathbf{m}_2$ vector (the cluster magnetic moment in the first excited state). The lowest level crossing of excited states with the ground state at $H = 0.21$ T is marked with an arrow.

is $H_{\min} = E_{20}/\mu m_2 = 0.21$ T. The field is directed along the $\mathbf{m}_2$ vector and causes the crossing of the degenerate $E_1 = E_9 = 0$ level with the nondegenerate $E_2(H)$ level. In spite of the degeneracy removal, the expected value of the toroidal moment in the cluster

$$\tau = \frac{\sum_{n=1}^{8} \tau_n e^{-E_{n0}/k_BT} \sinh(\mu \mathbf{m}_n \mathbf{H}/k_BT)}{\sum_{n=1}^{8} e^{-E_{n0}/k_BT} \cosh(\mu \mathbf{m}_n \mathbf{H}/k_BT)}$$

remains zero regardless of the external field magnitude and direction, as is easily seen from the data given in Table I. The states with nonzero expected values of the toroidal moment can be produced if the Hamiltonian in Eq. (1) contains nondiagonal terms, as will be shown in Sec. V.

As for the magnetic properties of the Dy_4 cluster, the dependencies of the magnetization vector components on the field magnitude and direction and the temperature can easily be analyzed by making use of Eqs. (2) and (3). The results, given by

$$\mathbf{m} = \frac{\sum_{n=1}^{8} \mathbf{m}_n e^{-E_{n0}/k_BT} \sinh(\mu \mathbf{m}_n \mathbf{H}/k_BT)}{\sum_{n=1}^{8} e^{-E_{n0}/k_BT} \cosh(\mu \mathbf{m}_n \mathbf{H}/k_BT)},$$

are shown in Figs. 4 and 5.

IV. MAGNETOELECTRICITY OF THE Dy_4 CLUSTER

In this section, we should consider the magnetoelectric interactions in the Dy_4 cluster. The electronic mechanism of the magnetoelectricity in rare-earth ions has already been outlined in Ref. [23]. We would like to discuss it somewhat closer in respect to the cluster.

Let a rare-earth ion be under the influence of external magnetic and electric fields. The actual perturbation Hamiltonian $\mathcal{V}_j$ of the jth ion then reads

$$\mathcal{V}_j = -\mathbf{d}_j \mathbf{E} + \mathcal{V}_{\text{cr}}^{\text{odd}}(j), \tag{4}$$

where $\mathbf{d}_j = -e \sum_{k=1}^{N} \mathbf{r}_k(j)$ is the dipole moment operator of the jth ion with $N = 9$ electrons in the $4f$ shell and $\mathbf{r}_k(j)$ is the radius vector of the kth $4f$ electron of the jth ion. Provided that the XY plane in Fig. 1 is a symmetry plane, the crystal field operator $\mathcal{V}_{\text{cr}}^{\text{odd}}(j)$ can be represented as

$$\mathcal{V}_{\text{cr}}^{\text{odd}}(j) = B_1^1(j)\left[\mathcal{C}_{-1}^1(j) - \mathcal{C}_1^1(j)\right] + B_0^1(j)\mathcal{C}_0^1(j). \tag{5}$$

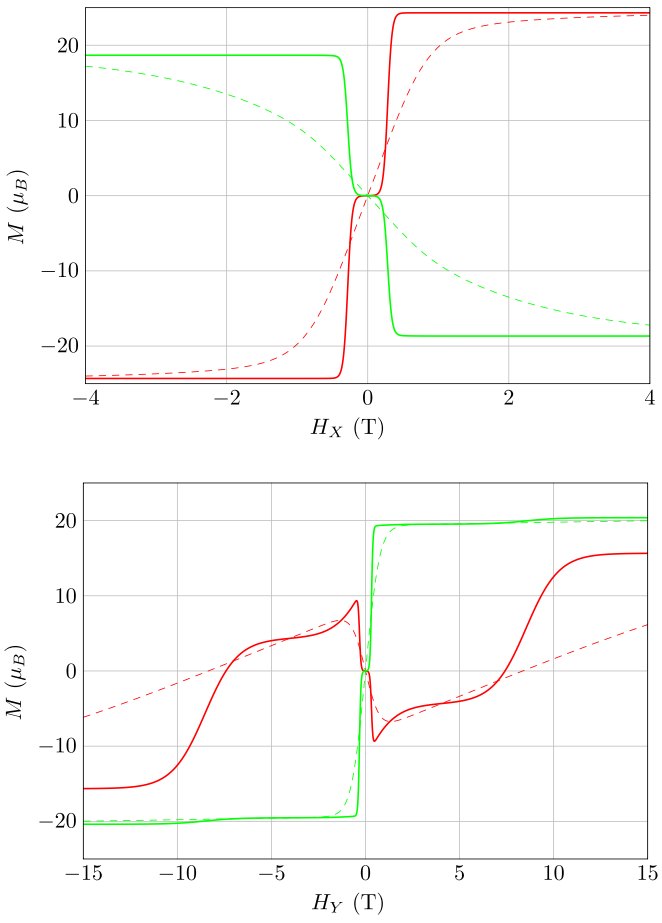

FIG. 4. The dependencies of the Dy_4 cluster magnetic moment M_X (red curves) and M_Y (green curves) on the field H for the cases $\mathbf{H}||OX$ (top) and $\mathbf{H}||OY$ (bottom) at the temperatures $T = 0.5$ K (the thicker solid curves) and $T = 4.2$ K (the thinner dashed curves).

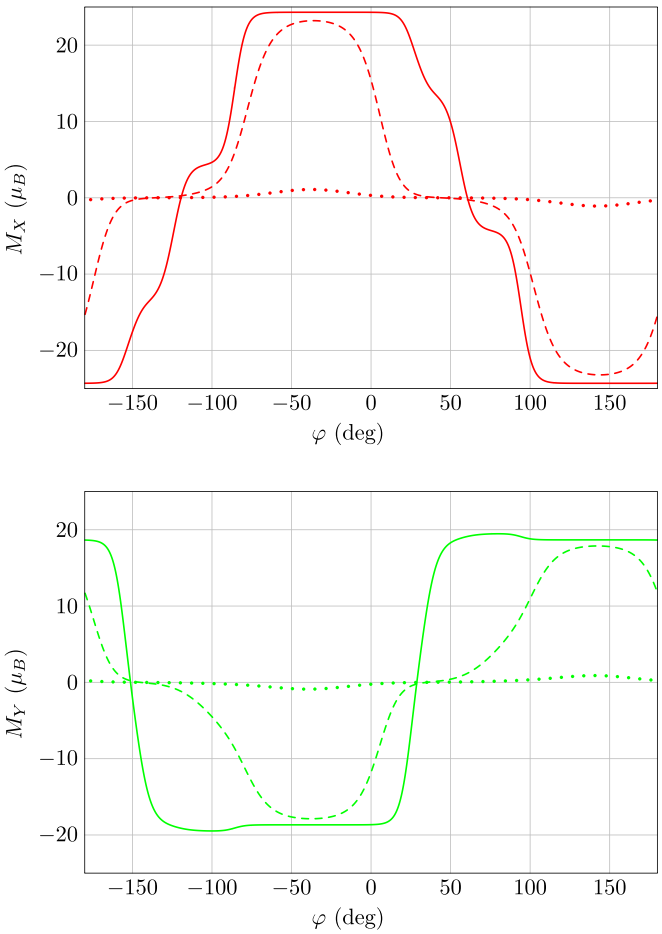

FIG. 5. The orientational dependencies of M_X (red curves of the upper graph) and M_Y (green curves of the lower graph) in the fields $H = 0.15$ T (field below the first level crossing at 0.21 T, the dotted curves), $H = 0.3$ T (dashed curves), and $H = 0.6$ T (solid curves) at the temperature $T = 0.5$ K. The magnetic moment is measured in the μ_B units. The φ angle between the **H** vector and the laboratory OX axis is measured in degrees.

Here $\mathcal{C}^1_q(j) = \sum_k \mathcal{C}^1_q(j,k)$, where $\mathcal{C}^1_q(j,k)$ are the single-electron irreducible tensor operators of the kth electron of the jth dysprosium ion.

In the $\mathbf{e}_\alpha(j)$ local coordinate axes, coefficients $B^1_q(j)$ are the parameters of the odd crystal field of the jth dysprosium ion. Due to symmetry, $B^1_q(1) = B^1_q(3)$ and $B^1_q(2) = B^1_q(4)$. Unfortunately, information on values of odd crystal field parameters for rare-earth ions is currently scarce. The parameters for praseodymium ions in ferroborate $PrFe_3(BO_3)_4$ are calculated in the frame of the point charge model [31]. They reach a value of 2.2×10^3 cm^{-1}. On the base of the parameter set it is possible to obtain the quantitative description of magnetoelectric properties of rare-earth iron [18] and aluminium [32] borates.

The corrections to the ion energy levels that linearly depend on the strength of the applied electric field arise in the second-order perturbation theory with small parameter $||\mathcal{V}||/W$, where $||\mathcal{V}||$ is the norm of the $\mathcal{V}$ operator and W is the energy difference between the ground states and the weight center of excited ion electronic configurations (typically, $W \sim 10^5$ cm^{-1} for rare-earth ions).

Making use of the wave function genealogical scheme and the quantum theory of angular momentum [33], we derive the expression for the effective Hamiltonian of the magnetoelectric interactions in the Dy_4 cluster,

$$\mathcal{H}_{\rm me} = \sum_{j=1}^{4} \mathcal{H}_{\rm me}(j), \tag{6}$$

where

$$\begin{aligned}\mathcal{H}_{\rm me}(j) = {} & E_x(j)\{b^1_1(j)[\mathcal{C}^2_{-2}(j) + \mathcal{C}^2_2(j) - \sqrt{\tfrac{2}{3}}\mathcal{C}^2_0(j)] \\ & + b^1_0(j)[\mathcal{C}^2_{-1}(j) - \mathcal{C}^2_1(j)]\} + \\ & + iE_y(j)\{b^1_1(j)[\mathcal{C}^2_{-2}(j) - \mathcal{C}^2_2(j)] \\ & + b^1_0(j)[\mathcal{C}^2_{-1}(j) + \mathcal{C}^2_1(j)]\} + \\ & + E_z(j)\{b^1_1(j)[\mathcal{C}^2_{-1}(j) - \mathcal{C}^2_1(j)] \\ & + \sqrt{\frac{8}{3}}b^1_0(j)C^2_0(j)\}.\end{aligned}$$

Note that $b^1_1(j) = -\sqrt{2}aB^1_1(j)$ and $b^1_0(j) = -aB^1_0(j)$, where $a = \sqrt{\frac{3^3}{2^3\times 5\times 7}}\frac{er_{fd}}{W}$, $r_{fd} = \langle f|r|d\rangle$ is the radial integral ($r_{fd} \sim 0.05$ nm for a Dy^{3+} ion [34,35]), and $W \sim 10^5$ cm^{-1}.

The ground state of a dysprosium ion in the Dy_4 cluster is a doublet that is very close to the $|\pm 15/2\rangle$ states (relative to the local symmetry axes). The excited doublet $|\pm 13/2\rangle$ is well separated from the ground one by the gap $\Delta \sim 200$ cm^{-1}. The external magnetic field mixes states $|\pm 13/2\rangle$ with states $|\pm 15/2\rangle$, thus making the ground states of the jth dysprosium ion in the field

$$|g^{(j)}_\pm\rangle = \left|\pm\frac{15}{2}\right\rangle - \frac{\mu\left(H^{(j)}_x \pm iH^{(j)}_y\right)}{\Delta\sqrt{15}}\left|\pm\frac{13}{2}\right\rangle.$$

In this case, the bilinear on E and H diagonal matrix element of the magnetoelectric Hamiltonian in Eq. (6) read

$$\begin{aligned}&\langle g_\pm(j)|\mathcal{H}_{\rm me}(j)|g_\pm(j)\rangle \\ &\quad = \pm A\left[b^1_1(j)H^{(j)}_x E^{(j)}_z + b^1_0(j)\left(H^{(j)}_x E^{(j)}_x + H^{(j)}_y E^{(j)}_y\right)\right],\end{aligned}$$

where $A = -14\sqrt{\frac{3}{2}}\frac{\mu\alpha_2}{\Delta}$, $\alpha_2 = -2/(5\times 7\times 9)$ is the second-order Stevens coefficient [36] for a Dy^{3+} ion. With this, we can obtain the bilinear corrections to the energies of the dysprosium cluster,

$$\begin{aligned}\delta E_n(H,E) = A\sum_j \sigma_j(n)b_j\big[&H^{(j)}_x E^{(j)}_z\cos\theta_j \\ &+ \left(H^{(j)}_x E^{(j)}_x + H^{(j)}_y E^{(j)}_y\right)\sin\theta_j\big],\end{aligned}$$

where $b_j = \sqrt{[b^1_1(j)]^2 + [b^1_0(j)]^2}$, $\cos\theta_j = b^1_1(j)/b_j$, and $\sin\theta_j = b^1_0(j)/b_j$.

By means of the function

$$\begin{aligned}&I(H,E,\theta,\varphi) \\ &\quad = H_z E_z\sin\theta + (H_x E_x\sin\varphi - H_y E_x\cos\varphi)\cos(\theta-\varphi) \\ &\qquad - (H_x E_y\sin\varphi - H_y E_y\cos\varphi)\sin(\theta-\varphi),\end{aligned}$$

one finds for the spin configurations shown in Fig. 2 that

$$\begin{aligned}
\delta E_1^{\mathrm{me}} &= 2A[b_1 I(H,E,\theta_1,\delta) + b_2 I(E,H,\theta_2,\pi/2+\gamma)],\\
\delta E_2^{\mathrm{me}} &= 0,\\
\delta E_3^{\mathrm{me}} &= 2Ab_1 I(H,E,\theta_1,\delta),\\
\delta E_4^{\mathrm{me}} &= -\delta E_3^{\mathrm{me}},\\
\delta E_5^{\mathrm{me}} &= 2Ab_2 I(H,E,\theta_2,\pi/2+\gamma),\\
\delta E_6^{\mathrm{me}} &= -\delta E_5^{\mathrm{me}},\\
\delta E_7^{\mathrm{me}} &= 2A[b_1 I(H,E,\theta_1,\delta) - b_2 I(H,E,\theta_2,\pi/2+\gamma)],\\
\delta E_8^{\mathrm{me}} &= 0.
\end{aligned} \tag{7}$$

For the other configurations with $\sigma_i(n') = -\sigma_i(n)$ $(n' = n+8)$ the corrections $\delta E_{n'}$ are opposite in sign. Supposed that $\delta = \gamma = 0$, $\theta_1 = \theta_2 = \theta$, and $b_1 = b_2 = b$, the expressions for the corrections to the levels of the ground doublet can be rewritten in a quite simple form,

$$\begin{aligned}
\delta E_{1,9} = \pm 2Ab[&(2H_z E_z + H_y E_y + H_x E_x)\sin\theta\\
&+ [\mathbf{H}\times\mathbf{E}]_z \cos\theta].
\end{aligned} \tag{8}$$

The components of the polarization vector **P** can be calculated on the basis of Eqs. (7) and (2). Here, we should note, that due to the specific structure of energy levels, the magnetoelectric effect is expected to be substantial at very low temperatures $(T \to 0)$, and then the levels of the split ground doublet are differently populated. The field and temperature dependencies of the polarization can be obtained provided that the set of the $\theta_{1,2}$, δ, γ, and $b_{1,2}$ parameters is known.

In the weak magnetic field the ground state of the Dy_4 complex is the degenerate state formed by spin configurations 1 and 9 (see Fig. 2). Spin-electric interaction removes the degeneration, thus making the ground state of the Dy_4 complex be a doublet with energies given by Eq. (8). The expressions contain a term (in the case $\theta = 0$ the only term)

$$\delta E = \pm(2Ab/T_0)(\mathbf{T}\cdot[\mathbf{E}\times\mathbf{H}]).$$

Remember that **T** stands here for the toroidal moment, $T_z/T_0 = \tau_z$; see Sec. 2. If the temperature tends to zero then the induced electric polarization is

$$\mathbf{P} = (2Ab/T_0)[\mathbf{H}\times\mathbf{T}], \tag{9}$$

which is consistent with general expression $\mathbf{P} \sim [\mathbf{H}\times\mathbf{T}]$, derived in Refs. [37,38] on the base of space-time symmetry considerations. Thus, it is possible to state that the magnetoelectricity of the system under consideration (at least in part) is reasoned by the toroidal nature of the Dy_4 molecule.

To estimate the value of the magnetoelectric effect, it is necessary to calculate the A and b constants, $1/A \sim 200$ T and $b \sim 5 \times 10^{-32}$ C m, and thus the corrections δE_i^{me} to the energy levels given by Eq. (7) reach the values of $\delta E_i^{\mathrm{me}} \sim 0.03\ \mathrm{cm}^{-1}$ in the fields $H \sim 1$ T and $E \sim 10^7$ V/cm. The electric dipole moment per molecule is then estimated to be up to $p \sim 10^{-4}$ D. It can be inferred from the supplementary materials for Ref. [20] that every cubic centimeter contains 6.22×10^{20} Dy_4 molecules, which means that the expected value of the Dy_4 molecular crystal polarization should reach 170 nC/m^2 in a 1-T magnetic field. The magnetoelectric constant α, defined as $P_i = \frac{1}{4\pi}\alpha_{ij}H_j$, is then estimated to be 5×10^{-5}. The α constant is comparable with that of the Dy_3 cluster [25] and even a half order more. In order to get a more substantial magnetoelectric effect, one should maximize the toroidal moment by coupling the Dy_3 clusters [39]. The magnetoelectricity of the coupled resulting Dy_6 cluster deserves a separate study.

There is also a nice possibility of the magnetoelectric effect existence driven by the interaction between the toroidal moment of the Dy_4 cluster and electric current (which can be a displacement current induced by a time-dependent external electric field). The energy of the interaction is $W = -\frac{4\pi}{c}(\mathbf{jT})$, where **j** is the density of the current running through the cluster. Such a current removes the degenerations of the ground doublet in a controlled manner and thus provokes the magnetoelectric effect to exist. The value of the effect depends on the rate of an external electric field change.

We should also note that there is an intriguing possibility to observe the nonequilibrium quantum MEE in the Dy_4 cluster. According to Ref. [20], the molecular cluster demonstrates the slow relaxation behavior, and the lifetime of the ground states limited by the macroscopic quantum tunneling can be as long as 0.1 s at 5 K. This empowers the observation of the quantum linear MEE in a single molecule with a probe field H, thus making the Pierre Curie's old idea on magnetoelectricity of molecules come true. Unlike the classical MEE, the quantum MEE will decay in time (or even oscillate) due to macroscopic quantum tunneling.

V. THE TOROIDAL MOMENT DYNAMICS

It is appropriate to recall that the above consideration was based on the exchange Hamiltonian, see Eq. (1), which is formulated under the Ising approximation, $g_x = g_y = 0$, $g_z \neq 0$. But, as follows from Ref. [20], the components g_x and g_y of the $\hat{g}$ tensor, though quite small $(g_{x,y} < 0.05)$, are yet nonzero. In this section, we go beyond this approximation, taking into account the behavior of the dysprosium ion magnetic moment as distinct from that within the limits of the Ising model. It is important for the adequate description of the toroidal moment dynamics. To do so, we introduce the nondiagonal terms added to the $\mathcal{H}_0$ Hamiltonian given by Eq. (1),

$$\mathcal{H} = \mathcal{H}_0 + \mathcal{H}_1 = \mathcal{H}_0 + \Delta\sum_{i=1}^{4} S_{ix}, \tag{10}$$

where S_{ix} are the projection operators of the effective spin onto the $\mathbf{e}_x(i)$ local axes. The operators can be expressed in terms of σ_{ix} Pauli matrices, $S_{ix} = \frac{1}{2}\sigma_{ix}$. The effective exchange constants J_i $(i = 1\ldots4)$ are cited from Ref. [20]; see Sec. II.

The last term in Eq. (10) can be treated as the influence of an external magnetic field directed perpendicular to the plane formed by the dysprosium ions, i.e., $\Delta = \mu_B g_x H$, where $g_x \neq 0$ is the small component of the g tensor of the dysprosium ion ground doublet. If $g_x < 0.05$ and $H \sim 1$ T, then Δ is estimated to be 0.023 cm^{-1}.

TABLE II. The matrix of the Dy_4 cluster Hamiltonian $\mathcal{H} = \mathcal{H}_0 + \mathcal{H}_1$ in the basis of the $\{\psi_i, \bar{\psi}_i\}$, $i = 1...8$, eigenvectors [see Eq. (11)]; $\delta = \Delta/2\sqrt{2}$ is the small parameter.

	ψ_1	$\bar{\psi}_1$	ψ_2	$\bar{\psi}_2$	ψ_3	$\bar{\psi}_3$	ψ_4	$\bar{\psi}_4$	ψ_5	$\bar{\psi}_5$	ψ_6	$\bar{\psi}_6$	ψ_7	$\bar{\psi}_7$	ψ_8	$\bar{\psi}_8$
ψ_1	0	0	2δ	0	2δ	0	0	0	0	0	0	0	0	0	0	0
$\bar{\psi}_1$		0	0	2δ	0	2δ	0	0	0	0	0	0	0	0	0	0
ψ_2			E_{30}	0	0	0	0	0	0	0	δ	δ	2δ	0	δ	δ
$\bar{\psi}_2$				E_{30}	0	0	0	0	0	0	δ	δ	0	2δ	δ	δ
ψ_3					E_{40}	0	0	0	0	0	δ	δ	0	2δ	δ	δ
$\bar{\psi}_3$						E_{40}	0	0	0	0	δ	δ	2δ	0	δ	δ
ψ_4							E_{30}	0	0	0	$-\delta$	δ	0	0	δ	$-\delta$
$\bar{\psi}_4$								E_{30}	0	0	δ	$-\delta$	0	0	$-\delta$	δ
ψ_5									E_{40}	0	δ	$-\delta$	0	0	δ	$-\delta$
$\bar{\psi}_5$										E_{40}	$-\delta$	δ	0	0	$-\delta$	δ
ψ_6											E_{20}	0	0	0	0	0
$\bar{\psi}_6$												E_{20}	0	0	0	0
ψ_7													E_{50}	0	0	0
$\bar{\psi}_7$														E_{50}	0	0
ψ_8															E_{60}	0
$\bar{\psi}_8$																E_{60}

In the case of $\Delta = 0$ the eigenenergies E_{n0} and the corresponding eigenstates ψ_n (the spin configurations) are

$$\begin{aligned}
\psi_1 &= |++++\rangle, \quad E_{10} = 0\ \mathrm{cm}^{-1},\\
\psi_{2,4} &= \frac{|+-++\rangle \pm |+++-\rangle}{\sqrt{2}}, \quad E_{30} = 3.033\ \mathrm{cm}^{-1},\\
\psi_{3,5} &= \frac{|-+++\rangle \pm |++-+\rangle}{\sqrt{2}}, \quad E_{40} = 3.365\ \mathrm{cm}^{-1},\\
\psi_6 &= |-++-\rangle, \quad E_{20} = 2.967\ \mathrm{cm}^{-1},\\
\psi_7 &= |+-+-\rangle, \quad E_{50} = 5.639\ \mathrm{cm}^{-1},\\
\psi_8 &= |--++\rangle, \quad E_{80} = 6.191\ \mathrm{cm}^{-1}.
\end{aligned} \tag{11}$$

Here symbols + and − stand for the projection signs of the ith dysprosium ion onto the local z_i axis. The conjugate $\bar{\psi}_n$ states differ from the ψ_n states in all the signs. The set of the vectors $\{\psi_1, \bar{\psi}_1, \ldots, \psi_8, \bar{\psi}_8\}$ forms the basis in the sixteen-dimensional Gilbert space. The matrix of Hamiltonian (10) in this basis is given in Table II. Clearly, $\mathcal{H}_{ik} = \mathcal{H}_{ki}$.

The two lowest eigenstates (the ground doublet with the splitting of 1.2×10^{-8} cm^{-1}) are $\Psi_1 = 0.688\psi_1 + 0.726\bar{\psi}_1$ and $\Psi_2 = 0.726\psi_1 - 0.688\bar{\psi}_1$; each of them is the superposition of the states very close to the states with $T_Z = \pm T_{\max}$, i.e., $\Psi_{1,2} = (\psi_+ \pm \psi_-)/\sqrt{2}$, where $\psi_+ \approx \psi_1$ and $\psi_- \approx \bar{\psi}_1$. The expected values of the toroidal moment in these states are $\langle\psi_\pm|\mathcal{T}_Z|\psi_\pm\rangle = \pm(1 - 1.5 \times 10^{-3})T_{\max}$.

Suppose that the system is initially in the ψ_+ state; then the probability $P(t)$ of finding it in the ψ_- state at time moment t is

$$\begin{aligned}
P(t) &= |\langle\psi_-|\psi_t\rangle|^2\\
&= \left|\sum_{n=1}^{16}\langle\Psi_n|\psi_-\rangle\langle\psi_+|\Psi_n\rangle \exp\left(-\frac{i}{\hbar}E_n t\right)\right|^2,
\end{aligned}$$

where $|\psi_t\rangle = \exp(-\frac{i}{\hbar}\mathcal{H}t)|\psi_+\rangle$. The probability $P(t)$ function oscillates (see Fig. 6), giving clear evidence of macroscopic quantum tunneling of the toroidal moment in the system. Similar oscillations of the magnetic moment in V_{15} single molecular magnets have already been observed [40].

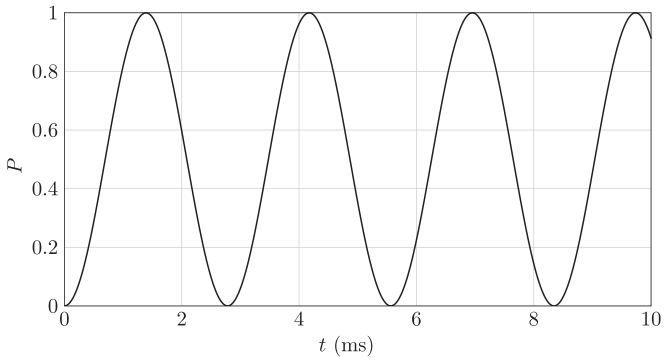

FIG. 6. Rabi-type oscillations between states $|\pm T_{\max}\rangle$; the plot shows the probability for the system to be in the $|-T_{\max}\rangle$ state.

The eigenfunctions are sought as expansion over the basis,

$$\Psi_\lambda = \sum_{k=1}^{8}(c_k\psi_k + \text{c.t.}),$$

where abbreviation c.t. stands for the conjugated terms. For the ground state ($\lambda \sim 0$) from the equation $(\mathcal{H}_{ik} - \lambda\delta_{ik})c_k = 0$ we find that $c_4 = c_5 = 0$, $c_6 = -\frac{\delta}{E_{20}-\lambda}(c_2 + c_3 + \text{c.t.})$, $c_8 = -\frac{\delta}{E_{60}-\lambda}(c_2 + c_3 + \text{c.t.})$, $c_7 = -\frac{2\delta}{E_{50}-\lambda}(c_2 + \bar{c}_3)$. Our task is to express all the c_k and $\bar{c}_k$ coefficients in terms of c_1 and $\bar{c}_1$, which can be found from the ground-state splitting. We will stick to the approximation $c_2 = c_2^0 + c_2'$ and $c_3 = c_3^0 + c_3'$, where $|c_{2,3}'| \ll |c_{2,3}^0|$. Under this approximation we find,

$$\begin{aligned}
c_2^0 &= -\tfrac{2\delta}{E_{30}}c_1, \quad c_2' = -\tfrac{8\delta^3}{E_{30}}B_E(c_1,\bar{c}_1),\\
c_3^0 &= -\tfrac{2\delta}{E_{40}}c_1, \quad c_3' = -\tfrac{8\delta^3}{E_{40}}B_E(c_1,\bar{c}_1),
\end{aligned}$$

where

$$\begin{aligned}
B_E(c_1,\bar{c}_1) = \frac{c_1+\bar{c}_1}{2}&\left(\frac{1}{E_{20}}+\frac{1}{E_{60}}\right)\left(\frac{1}{E_{30}}+\frac{1}{E_{40}}\right)\\
&+\frac{1}{E_{50}}\left(\frac{c_1}{E_{30}}+\frac{\bar{c}_1}{E_{40}}\right).
\end{aligned}$$

For the the c_1 and $\bar{c}_1$ coefficients we arrive to the system,

$$\begin{aligned}
(V_{11} - \lambda)c_1 + V_{1\bar{1}}\bar{c}_1 = 0,\\
V_{\bar{1}1}c_1 + (V_{11} - \lambda)\bar{c}_1 = 0,
\end{aligned}$$

where

$$\begin{aligned}
V_{11} = -4\delta^2&\left(\frac{1}{E_{30}}+\frac{1}{E_{40}}\right) - 8\delta^4\left(\frac{1}{E_{20}}+\frac{1}{E_{60}}\right)\\
&\times\left(\frac{1}{E_{30}}+\frac{1}{E_{40}}\right)^2 - \frac{16\delta^4}{E_{50}}\left(\frac{1}{E_{30}^2}+\frac{1}{E_{40}^2}\right),\\
V_{\bar{1}1} = V_{1\bar{1}} = -8\delta^4&\left[\left(\frac{1}{E_{20}}+\frac{1}{E_{60}}\right)\left(\frac{1}{E_{30}}+\frac{1}{E_{40}}\right)^2\right.\\
&\left.+\frac{4}{E_{30}E_{40}E_{50}}\right].
\end{aligned}$$

Nontrivial solutions of the system exist if $\lambda_{1,2} = V_{11} \pm V_{1\bar{1}}$, which gives the level splitting of $\Delta E = 2|V_{1\bar{1}}| \sim \delta^4$. For the lower state of the ground doublet $c_1 = \bar{c}_1 = 1/\sqrt{2}$ and for the upper state of the ground doublet $c_1 = -\bar{c}_1 = 1/\sqrt{2}$.

VI. CONCLUSION

In conclusion, the present analysis reveals that chirality of antiferromagnetic rare-earth nanoclusters with Ising-like magnetic anisotropy leads to the occurrence of the toroidal moment that allows specific spin-electric interactions and quantum magnetoelectric effect in them. The resulting quantum structure of nanocluster is rather rich and versatile to be manipulated by external electric and magnetic fields or just by current. Although we have considered mainly the specific rare-earth nanocluster, namely the Dy_4, many results can be applicable to other Ising-like lanthanide nanoclusters, e.g., Tb_4, Ho_4, etc. The rare-earth spin rings might be the best candidates to observe the quantum MEE in molecules as well as other peculiar spin-electric effects owing to their spin toroidal ground state with long relaxation time. Our study suggests that in rare-earth nanoclusters a spin chirality and an anapole moment are essential parameters in realizing a nanoscale quantum computing device.

ACKNOWLEDGMENTS

We wish to acknowledge the financial support of the Russian Foundation for Basic Research (Project No. 15-02-08509) and the Ministry of Education and Science of the Russian Federation (Project No. 2528).

[1] A. O. Caldeira and A. J. Leggett, Influence of Dissipation on Quantum Tunneling in Macroscopic Systems, Phys. Rev. Lett. **46**, 211 (1981).

[2] J. R. Friedman, M. P. Sarachik, J. Tejada, and R. Ziolo, Macroscopic Measurement of Resonant Magnetization Tunneling in High-Spin Molecules, Phys. Rev. Lett. **76**, 3830 (1996).

[3] R. Sessoli, D. Gatteschi, A. Caneschi, and M. A. Novak, Magnetic bistability in a metal-ion cluster, Nature (London) **365**, 141 (1993).

[4] L. Thomas, F. Lionti, R. Ballou, D. Gatteschi, R. Sessoli, and B. Barbara, Macroscopic quantum tunnelling of magnetization in a single crystal of nanomagnets, Nature (London) **383**, 145 (1996).

[5] V. V. Dobrovitski and A. K. Zvezdin, Macroscopic quantum tunnelling and hysteresis loops of mesoscopic magnets, Europhys. Lett. **38**, 377 (1997).

[6] L. Bokacheva, A. D. Kent, and M. A. Walters, Crossover between Thermally Assisted and Pure Quantum Tunneling in Molecular Magnet Mn12-Acetate, Phys. Rev. Lett. **85**, 4803 (2000).

[7] D. Gattechi, R. Sessoli, and J. Villain, *Molecular Nanomagnets* (Oxford University Press, New York, 2006).

[8] F. Beron, M. A. Novak, M. G. F. Vaz, G. P. Guedes, M. Knobel, A. Caldeira, and K. R. Pirota, Macroscopic quantum tunneling of magnetization explored by quantum-first-order reversal curves, Appl. Phys. Lett. **103**, 052407 (2013).

[9] J. Tejada, E. M. Chudnovsky, E. del Barco, J. M. Hernandez, and T. P. Spiller, Magnetic qubits as hardware for quantum computers, Nanotechnology **12**, 181 (2001).

[10] M. Affronte, F. Troiani, A. Ghirri, A. Candini, M. Evangelisti, V. Corradini, S. Carretta, P. Santini, G. Amoretti, F. Tuna, G. Timco, and R. E. P. Winpenny, Single molecule magnets for quantum computation, J. Phys. D: Appl. Phys. **40**, 2999 (2007).

[11] M. N. Leuenberger and D. Loss, Quantum computing in molecular magnets, Nature (London) **410**, 789 (2001).

[12] L. K. Grover, Quantum Computers can Search Arbitrarily Large Databases by a Single Query, Phys. Rev. Lett. **79**, 4709 (1997).

[13] L. Bogani and W. Wernsdorfer, Molecular spintronics using single-molecule magnets, Nat. Mater. **7**, 179 (2008).

[14] J. Lehmann, A. Gaita-Arino, E. Coronado, and D. Loss, Spin qubits with electrically gated polyoxometalate molecules, Nat. Nanotechnol. **2**, 312 (2007).

[15] M. Trif, F. Troiani, D. Stepanenko, and D. Loss, Spin electric effects in molecular antiferromagnets, Phys. Rev. B **82**, 045429 (2010).

[16] S. Thiele, F. Balestro, R. Ballou, S. Klyatskaya, M. Ruben, and W. Wernsdorfer, Electrically driven nuclear spin resonance in single-molecule magnets, Science **344**, 1135 (2014).

[17] F. Troiani, A. Ghirri, M. Affronte, S. Carretta, P. Santini, G. Amoretti, S. Piligkos, G. Timco, and R. E. P. Winpenny, Molecular Engineering of Antiferromagnetic Rings for Quantum Computation, Phys. Rev. Lett. **94**, 207208 (2005).

[18] A. I. Popov, D. I. Plokhov, and A. K. Zvezdin, Quantum theory of magnetoelectricity in rare-earth multiferroics: Nd, Sm, and Eu ferroborates, Phys. Rev. B **87**, 024413 (2013).

[19] L. F. Chibotaru, L. Ungur, and A. Soncini, The origin of nonmagnetic Kramers doublets in the ground state of dysprosium triangles: Evidence for a toroidal magnetic moment, Angew. Chem. Int. Ed. **47**, 4126 (2008).

[20] P.-H. Guo, J.-L. Liu, Z.-M. Zhang *et al.*, The first Dy_4 single-molecule magnet with a toroidal magnetic moment in the ground state, Inorg. Chem. **51**, 1233 (2012). The supporting information can be found at http://pubs.acs.org/doi/suppl/10.1021/ic202650f

[21] L. Ungur, S. K. Langley, T. N. Hooper, B. Moubaraki, E. K. Brechin, K. S. Murray, and L. F. Chibotaru, Net toroidal magnetic moment in the ground state of a Dy_6 triethanolamine ring, J. Am. Chem. Soc. **134**, 18554 (2012).

[22] V. E. Campbell, H. Bolvin, E. Riviere, R. Guillot, W. Wernsdorfer, and T. Mallah, Structural and electronic dependence of the single-molecule-magnet behavior of dysprosium (III) complexes, Inorg. Chem. **53**, 2598 (2014).

[23] A. I. Popov, D. I. Plokhov, and A. K. Zvezdin, Anapole moment and spin-electric interactions in rare-earth nanoclusters, Europhys. Lett. **87**, 67004 (2009).

[24] D. I. Plokhov, A. K. Zvezdin, and A. I. Popov, Macroscopic quantum dynamics of toroidal moment in Ising-type rare-earth clusters, Phys. Rev. B **83**, 184415 (2011).

[25] D. I. Plokhov, A. I. Popov, and A. K. Zvezdin, Quantum magnetoelectric effect in the molecular cluster Dy_3, Phys. Rev. B **84**, 224436 (2011).

[26] L. Ungur, S.-Y. Lin, J. Tang, and L. F. Chibotaru, Single-molecule toroics in Ising-type lanthanide molecular clusters, Chem. Soc. Rev. **43**, 6894 (2014).

[27] D. N. Woodruff, R. E. P. Winpenny, and R. A. Layfield, Lanthanide single-molecule magnets, Chem. Rev. **113**, 5110 (2013).

[28] J. Tang and P. Zhang, *Lanthanide Single Molecule Magnets* (Springer-Verlag, Berlin, 2015).

[29] J. Luzon, K. Bernot, I. J. Hewitt, C. E. Anson, A. K. Powell, and R. Sessoli, Spin Chirality in a Molecular Dysprosium Triangle: The Archetype of the Noncollinear Ising Model, Phys. Rev. Lett. **100**, 247205 (2008).

[30] V. M. Dubovik and V. V. Tugushev, Toroid moments in electrodynamics and solid-state physics, Phys. Rep. **187**, 145 (1990).

[31] M. N. Popova, T. N. Stanislavchuk, B. Z. Malkin, and L. N. Bezmaternykh, Optical spectroscopy of $PrFe_3(BO_3)_4$: Crystal field and anisotropic Pr-Fe exchange interactions, Phys. Rev. B **80**, 195101 (2009).

[32] A. M. Kadomtseva, Yu. F. Popov, G. P. Vorob'ev, N. V. Kostyuchenko, A. I. Popov, A. A. Mukhin, V. Yu. Ivanov, L. N. Bezmaternykh, I. A. Gudim, V. L. Temerov, A. P. Pyatakov, and A. K. Zvezdin, High-temperature magnetoelectricity of terbium aluminum borate: The role of excited states of the rare-earth ion, Phys. Rev. B **89**, 014418 (2014).

[33] D. Varshalovich, A. Moskalev, and V. Khersonskii, *Quantum Theory of Angular Momentum* (World Scientific, Singapore, 1989).

[34] N. F. Vedernikov, A. K. Zvezdin, R. Z. Levitin, and A. I. Popov, Magnetic linear birefringence of rare-earth garnets, Zh. Eksp. Teor. Fiz. **93**, 2161 (1987) [Sov. Phys. JETP **66**, 1233 (1987)].

[35] B. R. Judd, Optical absorption intensities of rare-earth ions, Phys. Rev. **127**, 750 (1962).

[36] K. W. H. Stevens, Matrix elements and operator equivalents connected with the magnetic properties of rare-earth ions, Proc. Phys. Soc., London, Sect. A **65**, 209 (1952).

[37] N. A. Spaldin, M. Feibig, and M. Mostovoy, The toroidal moment in condensed-matter physics and its relation to the magnetoelectric effect, J. Phys.: Condens. Matter **20**, 434203 (2008).

[38] Yu. V. Kopaev, Toroidal ordering in crystals, Phys. Usp. **52**, 1111 (2009).

[39] S.-Y. Lin, W. Wernsdorfer, L. Ungur, A. K. Powell, Y.-N. Guo, J. Tang, L. Zhao, L. F. Chibotaru, and H.-J. Zhang, Coupling Dy_3 triangles to maximize the toroidal moment, Angew. Chem. Int. Ed. **51**, 1 (2012).

[40] S. Bertaina, S. Gambarelli, T. Mitra, B. Tsukerblat, A. Müller, and B. Barbara, Quantum oscillations in a molecular magnet, Nature (London) **453**, 203 (2008); see also the corrigendum, **466**, 1006 (2010).